Structural Effects on the Transport of Water in Polyimides

John G. Van Alsten* and John C. Coburn

Central Research & Development, E. I. du Pont de Nemours & Company, Experimental Station, Wilmington, Delaware 19880-0356

Received February 18, 1994; Revised Manuscript Received April 14, 1994®

ABSTRACT: The influence of molecular primary and secondary structure on the transport of water has been investigated for a series of chemically similar polyimides using an infrared ATR method. The diffusivity of water generally decreased with increased chain backbone stiffness (as determined from the mechanical β transition), and the activation energies for diffusion generally increased with backbone stiffness. For a given backbone composition, the diffusivity was also shown to markedly increase as the density of the amorphous phase decreased. The vibrational spectra show that the absorbed water partitions into a bimodal distribution of sites, presumably representing single and clustered water molecules. This distribution changes markedly with saturation and is hence a sensitive probe of the local heterogeneity of the glassy structure.

Polyimides are important materials for the electronics industry due to their thermal stability and relatively high dielectric strength. One recurrent issue with these materials is the facile transport of water through them; in solid state electronic devices this can lead to the formation of a hydrated inorganic/polymer interface and subsequent delamination and failure of the device. Consequently, a fairly substantial literature has developed regarding the transport[1] and state[2] of water in polyimide films.

Virtually all the studies to date have been concerned with the influence of backbone chemistry, or primary structure, on water transport. Most of these works set a standard cure protocol for the various compositions and have not been concerned with the morphological details of the films thereby prepared. Our own interests are the converse, namely to utilize very similar backbone chemistries but vary the cure procedures in a manner such that the relationship between transport and both the molecular primary and secondary structure may be investigated.

It is well-known that the structure of polyimide films is remarkably sensitive to the curing history. In previous work by Coburn and Pottiger,[3] it was shown that birefringence in spin coated films is dependent on the initial film thickness, the heating rate, and the final cure temperature. The development of crystallinity is also critically dependent on thermal history. These morphological details manifest themselves as variations in such important physical properties as the modulus, coefficient of thermal expansion, and the level of residual stress. To our knowledge, their effects on transport have not been addressed.

Experimental Section

Diffusion Measurements by ATR Spectroscopy. Diffusion measurements were obtained by the infrared attenuated total reflectance (ATR) method, which was first proposed and investigated by Hemmelman and Brandt[4] and has recently been applied by Fieldson and Barbari in a study of water diffusion in poly(acrylonitrile).[5] This technique uses infrared spectroscopy to monitor the uptake of penetrant into a polymer film that is in contact with an ATR element, which is fashioned from an infrared transmissive material of high refractive index such as zinc selenide or silicon. The technique selectively measures species within a reasonably short distance from the polymer/element interface. This distance is characterized by a penetration depth, λ, over which the magnitude of the interrogating electric field diminishes by a factor of $1/e$. The penetration depth of the evanescent wave can be evaluated from the expression[6]

$$\lambda = \frac{\lambda_1}{2\pi(\sin^2\theta - n_{21}^2)^{1/2}} \tag{1}$$

Here λ_1 is the wavelength of the infrared beam in the ATR element, θ the angle of incidence of the radiation at the polymer/element interface, and n_{21} the ratio of the refractive index of the polymer to that of the element. For typical materials and midinfrared wavelengths, λ is on the order of 0.1–1 μm.

To be useful in quantifying diffusion coefficients, it is necessary to relate the measured infrared absorbance to species concentration. In an ATR experiment, the measured absorbance is determined by the convolution of the species concentration profile and the exponentially weighted molar absorptivity:

$$A = \int_0^\infty \alpha \exp(-2x/\lambda) C(x) S \, dx \tag{2}$$

In this expression α is the characteristic oscillator strength, $C(x)$ the concentration profile, and S the interfacial area over which the measurement occurs. When the temporal dependence of the concentration profile is included by using a solution such as those found in Crank,[7] the time dependence of the measured absorbance becomes a route for the evaluation of diffusion coefficients. For the Fickian diffusion of a penetrant, where the polymer film thickness $L \gg \lambda$, this leads to

$$\frac{A}{A_\infty} = 1 - \frac{8}{\pi\lambda}\sum_{n=0}^{\infty}\frac{(-1)^n}{2n+1}\frac{1}{\frac{2}{\lambda} + \frac{(2n+1)^2\pi^2\lambda}{8L^2}\exp\left\{\frac{-D(2n+1)^2\pi^2 t}{4L^2}\right\}} \tag{3}$$

in which the diffusion coefficient D is the only adjustable parameter. Diffusion coefficients are consequently determined by fitting expression 3 to normalized experimental data.

Film Preparation and Characterization. Four all aromatic polyimides were utilized, benzophenonecarboxylic dianhydride//*p*-phenylenediamine (BTDA//PPD), biphenylcarboxylic dianhydride//*p*-phenylenediamine (BPDA//PPD), pyromellitic dianhydride//4,4′-oxydianiline (PMDA//ODA), and a copolymer of benzophenonecarboxylic dianhydride//4,4′-oxydianiline/*m*-phenylenediamine (BTDA//ODA/MPD). These are commercial compositions available from DuPont Electronics under the trade name Pyralin and are provided in the form of polyamic acids dissolved in *N*-methylpyrollidinone solvent. The backbone structures are shown in Figure 1. Poly(amic acid) films were prepared by spin coating the solutions directly onto the face of the silicon infrared attenuated total reflectance (ATR) crystals.

The as spun poly(amic acids) are converted to their corresponding polyimides by subsequent curing. The morphology

* Abstract published in *Advance ACS Abstracts*, June 1, 1994.

0024-9297/94/2227-3746$04.50/0

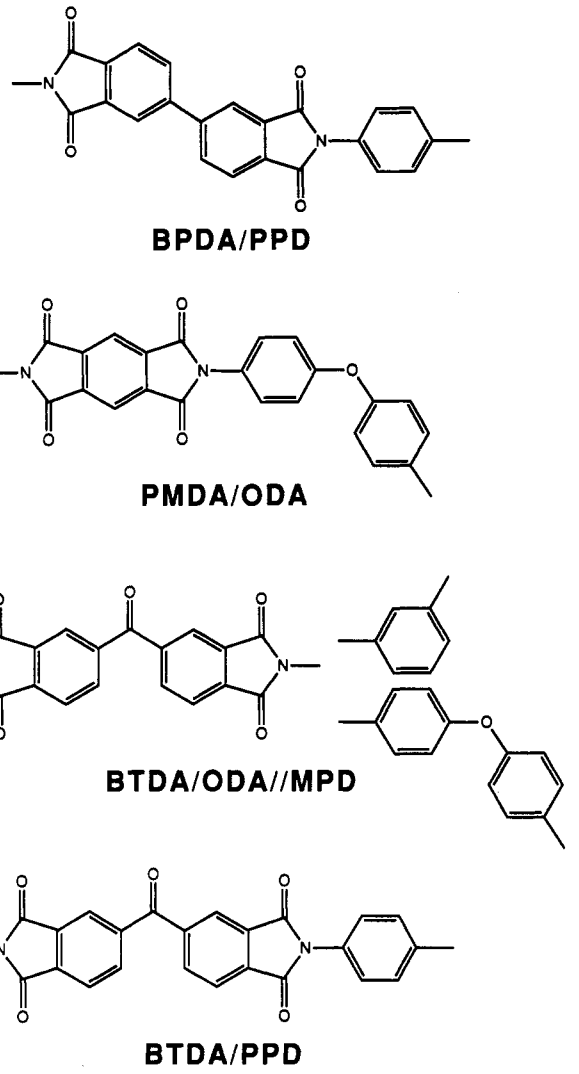

Figure 1. Backbone structures of the polyimides used in this study.

of each sample is determined by the particular curing cycle used to prepare the polyimide. All of the samples were first dried in an air oven at 135 °C for 30 min to remove solvent. Then, one of several baking procedures was applied in a nitrogen-purged furnace (Blue M Corp.):

-a ramp of 2 °C/min from 135 to 300, 350, or 400 °C, then held for 1 h

-placed directly into an oven at 300 °C for 1 h

-placed directly into an oven at 425 °C for 1 h

-a ramp of 2 °C/min from 135 to 300 °C, held 1 h, then placed directly in an oven at 425 °C for 1 h

The morphology of the films is very sensitive to the cure cycle used. Gardner[8] has established that temperatures in excess of 400 °C are necessary for the nucleation of crystallinity in these systems. In addition, the relative rates of heating determine the ultimate density of the amorphous phase. For rapid heatings, the polymer chains will spend some portion of time above their effective glass transition temperatures (which are dictated by the overall level of imidization and the quantity of residual solvent) and so form films of higher density than those heated more slowly, where the chains are always below the effective T_g's.

Prior to beginning a diffusion experiment the film index of refraction and birefringence were measured directly on the substrates with a Metricon Model 2000 integrated optics prism coupling waveguide system utilizing a HeNe laser (633 nm). Because the films were isotropic in the plane, only two refractive indices, the in-plane refractive index, n_{TE}, and the out-of-plane refractive index, n_{TM}, were needed to characterize the optical anisotropy in the films. The birefringence, Δn, was determined

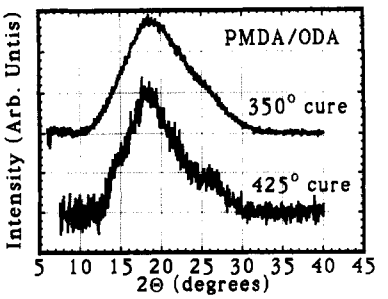

Figure 2. Reflection X-ray patterns from PMDA/ODA samples cured at different temperatures. The lower temperature cure gives a completely amorphous sample, while the cure at higher temperature produces a sample with ca. 12% crystallinity.

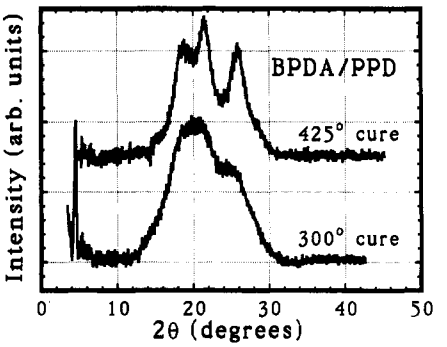

Figure 3. Reflection X-ray patterns from BPDA/ODA samples. The higher temperature cure results in a film ca. 42% crystalline.

from the difference between the in-plane and out-of-plane refractive indices. The prism coupling technique was also used to measure film thickness.

The birefringence of films adhered to crystals is a combination of the birefringence resulting from molecular orientation and the birefringence induced by the residual stress present in the films. Therefore, the measured birefringence includes both the intrinsic birefringence and the birefringence resulting from the stress-optical effect.[9]

When a series of runs had been completed, the films were carefully peeled from the silicon substrates and the densities determined using a gradient column made from a mixture of *n*-heptane and carbon tetrachloride. Reflection X-ray data (Figures 2 and 3) were also obtained for the PMDA/ODA and BPDA/PPD materials. Only the two films heated above 420 °C showed any evidence of crystalline scattering. These fractional crystallinities were determined by deconvolution. The BTDA/ODA//MPD copolymer is completely amorphous, and the BTDA/PPD polymer was inferred to be the same under the cure conditions used.

For the PMDA/ODA polymers, an ideal amorphous phase density can be estimated using the crystalline density, 1.48 g/cm^3,[8] the measured fractional crystallinity, and the measured density of the single semicrystalline sample. This results in an estimate for a dense amorphous phase of 1.42 g/cm^3. All of the samples prepared at low (<425 °C) ultimate temperatures have bulk densities below this value. This indicates that the thermal treatments used in these samples did not exceed the effective T_g's for a duration sufficient to densify the amorphous phase of these samples. Thus, solvent loss and volume changes on imidization are reflected as "extra" volume which persists in the final film.

We attempted to apply a similar analysis to the BPDA/PPD composition, which can be readily driven to reasonably high levels of crystallinity. Unfortunately, literature assignments of the crystalline space group[13] yield crystallite densities (1.408 g/cm^3) well below the densities measured on both the semicrystalline and amorphous films (1.4618 and 1.4472 g/cm^3, respectively) which renders impossible such an analysis.

Mechanical determinations of transitions were obtained using the thin film tensile mode of a Rheometrics RSA-II solids analyzer. Measurements were obtained on a free standing film. The transition temperatures were obtained from maxima in isochronal

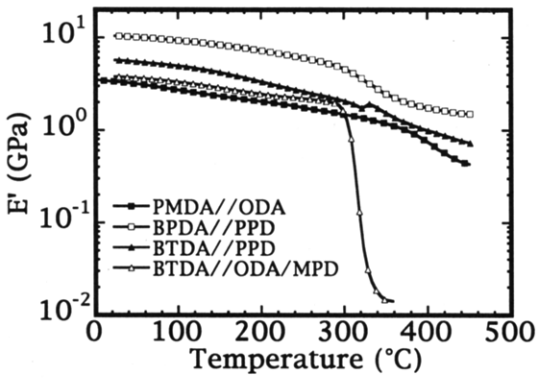

Figure 4. Dynamic tensile modulus isochronal (100 radians/s) curves as a function of temperature for PMDA//ODA, BPDA//PPD, BTDA//PPD, and BTDA//ODA/MPD (100//50/50).

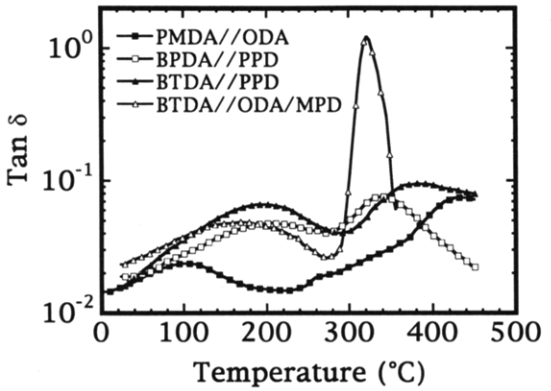

Figure 5. Dynamic tan δ (100 radians/s) curves as a function of temperature for PMDA//ODA, BPDA//PPD, BTDA//PPD, and BTDA//ODA/MPD (100//50/50). The high temperature transition corresponds to the glass transition. The low temperature (β) transition temperatures are reported in Table 2.

(i.e., 10 and 100 radians/s) tan δ vs temperature curves. Static pretension of 100 g and a 0.1% dynamic strain amplitude were used for the measurements. The dynamic tensile modulus and tan δ were acquired over a temperature range from 30 to 500 °C and are shown in Figures 4 and 5, respectively. Apparent activation energies were determined from the frequency dependence of the transition temperatures by assuming Arrhenius behavior.

Diffusion Measurements. For the experiments presented here, values of the penetration depth, λ, were calculated using a literature value of the refractive index of PMDA/ODA at 2600 cm^{-1} (1.68).[10] The silicon ATR crystals[11] were cut to provide a 60° angle of incidence. From eq 1, the penetration depth at 2600 cm^{-1} is 0.24 μm.

The polymer-coated ATR elements were mounted in the assembly shown in Figure 6, which consists of a fluid ATR cell (Harrick) equipped with leads for both circulating fluid and electrical cartridge heaters. In this manner, it is possible to thermostat the cell from approximately 0 to 400 °C. The cell assembly is mounted within the nitrogen-purged spectrometer (Nicolet Instruments 60SX) sample compartment, which has been modified to pass leads for thermostating fluid, resistive heating, and sample injection tubing. A Teflon valve and tubing manifold allows either the injection of liquid material or purging of high purity helium (MG Industries, 99.9995%) through the cell, with the purge outlet buried beneath a bed of $CaSO_4$ desiccant.

Experiments begin with a rigorous drying procedure in which the cell is heated under flowing helium first to 90 °C for 30 min and then to 150 °C for at least 2 h. The cell is then brought to the temperature of interest and allowed to equilibrate for approximately 1 h, and a run is commenced by injecting neat D_2O into the cell with simultaneous data acquisition. Spectral collection is performed automatically by the computer-controlled instrument. To optimize data acquisition, data collection is broken into early and late stages, with rapid scans performed at

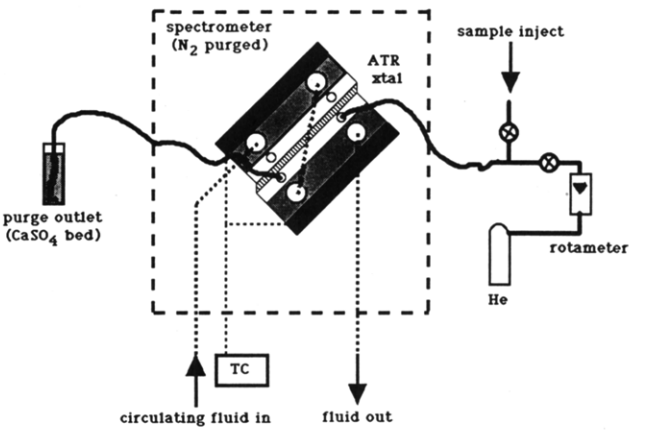

Figure 6. Schematic of the ATR diffusion cell. The polymer sample covers one side of a silicon ATR crystal, which is installed in a temperature controlled cell into which liquid or gas may be injected. This is mounted within the nitrogen-purged chamber of an FTIR spectrometer.

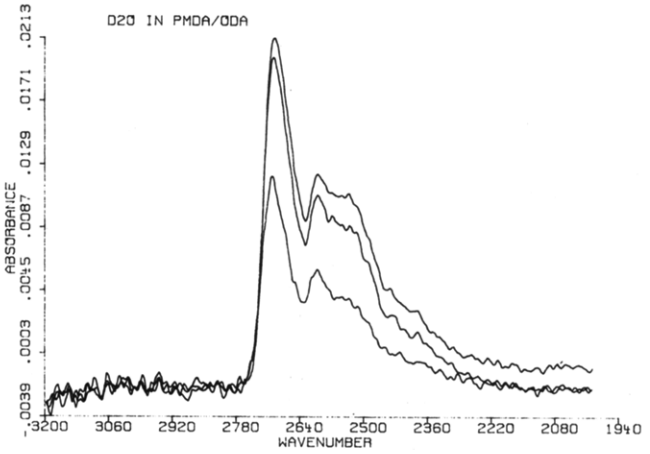

Figure 7. Infrared spectra of the O–D stretching region at three different times in an experiment. The sharp peak at high wavenumbers is considered to be monomeric D_2O, while the broad region at lower wavenumbers is considered to consist of aggregates of several D_2O molecules.

the beginning of the run and spectra with longer collection times at later stages. This allows a balance to be obtained between good temporal resolution and signal to noise. Typical spectral acquisition times using this approach range from ca. 2.5 to 25 s. Data were collected with 8-cm^{-1} resolution. Following a run, data are processed and the characteristic O–D stretching region (Figure 7) is integrated to obtain the mass of absorbed D_2O.

Upon completion of a run, the cell was purged of liquid water with flowing helium, and the drying cycle was repeated. To minimize possible effects of physical aging, experiments on each film were conducted in a sequence from the highest temperature (90 °C) to the lowest (5 °C).

Results

A typical uptake versus time plot for water into polyimide films is presented in Figure 8. As the inset to this figure shows, the data appear to plateau in a Fickian manner if plotted in a linear fashion. Plotting the data semilogarithmically, however, is much more informative. From this representation, it is seen that there is in fact no real plateau to the data but that the uptake appears to continue at a rate proportional to the logarithm of time. This proportionality decreases with increasing temperature, as illustrated in Figure 9. Yang et al.[1] have suggested that the hydrothermal aging of Kapton PMDA/ODA films may be due to incorporation of water into uncyclized poly(amic acid) residues. In our study, this would be clearly

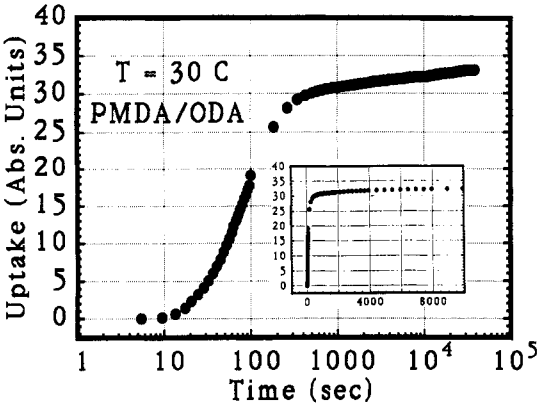

Figure 8. Typical uptake behavior for polyimide films in contact with D_2O, showing initially Fickian behavior followed by a slow increase in absorbed water. The inset displays the data plotted in a linear fashion. System: PMDA/ODA at 30 °C.

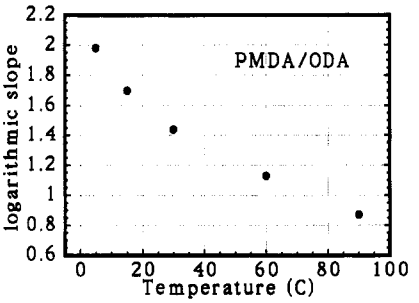

Figure 9. Slope of the uptake vesus logarithm of time for the "plateau" region of the uptake curve at five temperatures for a typical sample.

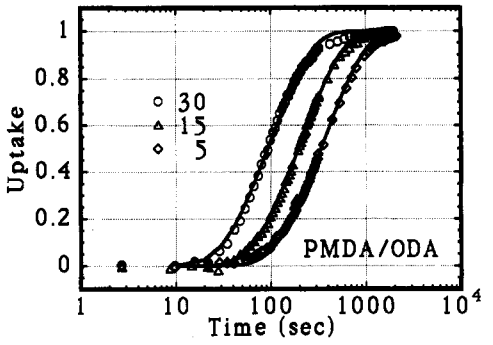

Figure 10. Normalized data showing typical goodness of fit to the theoretical expression for Fickian diffusion given in eq 3.

evidenced by a strong *negative* peak in the difference spectra in the N-H stretching region as hydrogen atoms were exchanged for deuterium. No such evidence was observed.

The fact that water continues to be absorbed through very long times also complicates the data analysis, since there is no true absorbance plateau with which to normalize the data. This issue has been finessed by normalizing the data by the value of the absorbance where the data begin the linear uptake with logarithmic time behavior. An example of data manipulated by this procedure is shown in Figure 10. Also displayed are typical fits of eq 3 to these normalized data. Over most of the experiment, the data are well fit by the Fickian model. Some departure from the model does begin near the uptake plateau—this region has been expanded in Figure 11. This undershoot was noted for every run of every sample tested and has been observed in previous studies of PMDA/ODA.[1] Unfortunately, we cannot be certain if this undershoot represents a real departure from Fickian behavior or is simply a manifestation of the normalization procedure

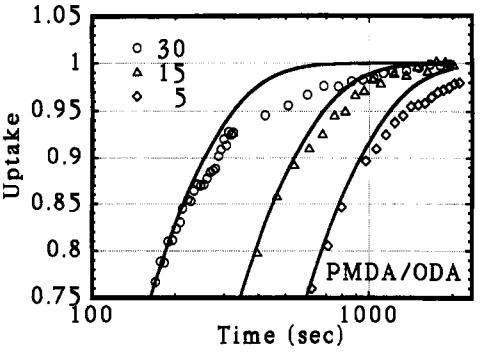

Figure 11. Illustration of the deviation from Fickian behavior at high levels of uptake.

that we have utilized. A summary of all the experimental data is given in Table 1.

Activation energies for diffusion were calculated in standard Arrhenius form by fitting the dependence of the logarithm of the diffusion coefficient on reciprocal temperature (Figure 12). These averaged 10.4 kcal/mol for BTDA/PPD, 9.5 kcal/mol for BPDA/PPD, 8.4 kcal/mol for PMDA/ODA, and 7.6 kcal/mol for BPDA/ODA//MPD, respectively. Our values lie within the spectrum of those previously reported for the PMDA/ODA polymer, which range from 5.4 to 10.3 kcal/mol.[1]

Important information is also available from the line shapes of the vibrational spectra. It is well-known that the infrared absorption bands of hydrogen bonding systems are very susceptible to perturbations from the surrounding environment, with characteristic red shifts occurring as hydrogen bond donors and acceptors share electron density.[12] The O–D stretch region of Figure 7 clearly shows the presence of at least two distinct domains in which the absorbed heavy water resides within the polymer. Furthermore, the relative line widths suggest that the high and low energy regions arise from D_2O molecules existing in isolated and clustered states, respectively.

The absorption bands also show a slight red shift as penetration by the heavy water proceeds. Figure 13 illustrates the red shift of the isolated O–D stretching frequency with time for an experiment with PMDA/ODA at 5 °C, which shows that the intimacy of association of D_2O molecules with sites on the polymer backbone is increasing as more D_2O is absorbed. By converting this red shift to energy via Planck's constant, this stabilization is approximately 66 kcal/mol.

If the high energy (wavenumber) peak line width is taken to be representative of a monomeric O–D stretch, the width of the low energy (wavenumber) region can be translated into an approximation of the number of distinct O–D environments this region represents. This simplistic analysis indicates that this region is composed of 3–4 overlapping O–D stretches. If the isolated and clustered states are assumed to contain exchangeable molecules, an equilibrium constant may be calculated:

$$K = C_n/C^n \tag{4}$$

In this expression, C is the concentration of isolated D_2O molecules and C_n the concentration of D_2O clusters of n molecules. Assuming equivalent infrared oscillator strength, this is equivalent to

$$K = \left[\frac{1-f_m}{n}\right]/[f_m]^n \tag{5}$$

where f_m is the fraction of the total peak area due to monomer and n is the number of O–D states in the cluster.

Table 1. Diffusion Coefficients and Structure (Diffusion Coefficients in $cm^2/s \times 10^9$)

	PMDA/ODA				BPDA/PPD		BTDA/ODA//PPD		
	A[a]	B	C	D	E	F	G	H	BTDA/PPD
temp (°C)									
5	1.0	1.8	1.6	2.6	0.052	0.062	1.9	1.6	0.16
15	2.0	3.2	3.1	4.5	0.097	0.10	3.3	3.5	0.28
30	4.2	7.7	7.5	9.5	0.22	0.32	6.0	5.2	0.66
60	14	26	25	32	x	1.2	19	13	3.2
90	37	57	63	95	x	3.6	30	20	13
E_a (kcal/mol)	8.39	8.23	8.53	8.44	9.64	9.43	7.69	7.66	10.4
ρ (g/cm³)	1.4244	1.408	1.4064	1.3917	1.4618	1.4472	1.3843	1.3830	
fractional extra vol	0	0.0057	0.0068	0.017					
Δn	0.0763	0.0661	0.0682	0.0698	0.2320	0.2028	-0.0029	0.0161	0.0997
cure	135 °C/ 30 min 425 °C "rapid"	135 °C/ 30 min 300 °C "rapid"	135 °C/ 30 min 400 °C "ramp"	135 °C/ 30 min 350 °C "ramp"	135 °C/ 30 min 300 °c/ 30 min 425 °C/ 60 min	135 °C/ 30 min 300 °C/ 60 min	135 °C/ 30 min 425 °C/ 60 min	135 °C/ 30 min 350 °C/ 60 min	135 °C/ 30 min 350 °C/ 60 min

[a] Data as listed have not been normalized by the amorphous phase volume fraction (0.88) of this sample.

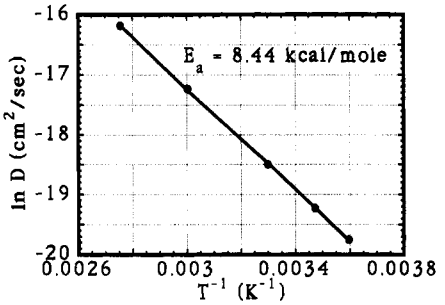

Figure 12. Typical fit of data to an Arrhenius expression. System: PMDA/ODA.

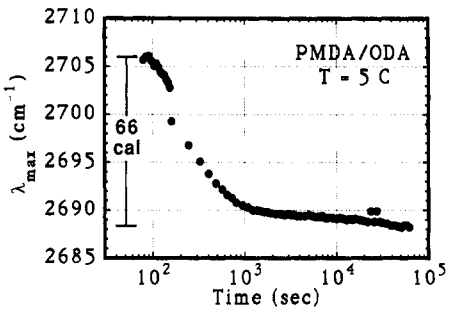

Figure 13. Red shift in the absorbance maximum with time, indicating that the intimacy of hydrogen bonding increases as the material becomes saturated with water. The total degree of stabilization is approximately 66 cal.

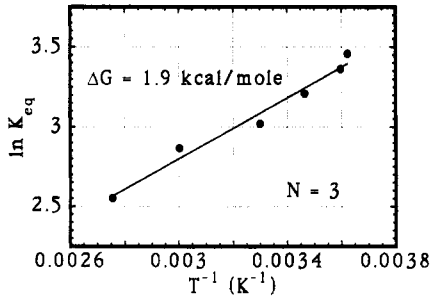

Figure 14. Evaluation of the free energy difference between the monomeric and aggregate states of absorbed D_2O. This particular model assumes that the water aggregates consist of three molecules.

It is then possible to determine the difference in the free energy between these two states from the change in the equilibrium constant with temperature. Figure 14 shows such an analysis by assuming a cluster size of 3 units, which gives an energy difference of 1.9 kcal/mol.

Table 2. β Transition Data

backbone	T_β (°C)	E_a (kcal/mol)
PMDA/ODA	104	37
BTDA/ODA//MPD	160	31
BTDA/PPD	195	35
BPDA/PPD	204	23

Table 2 presents the analysis applied for clusters of 2–5 units, with the results ranging from 1.3 to 3.0 kcal/mol.

Discussion

Departures from Fickian Transport. It is well-known that the diffusion behavior of small molecules in polymers should be Fickian well below the glass transition temperature of the host. It is therefore not surprising that Fickian behavior is observed in these materials, in which the experiments were all performed at least 200 deg below T_g. Some departure from this behavior is witnessed in the undershoot of the data at high uptakes, suggesting that the ease with which water molecules squeeze between chains does diminish at high water loadings. This may indicate that the sorbed water further constrains local chain motions necessary to permit penetrant molecules to move through the glass.

Effect of Crystallinity and Density. For small molecule penetrants, polymer crystallinity generally diminishes the overall coefficient of diffusion by a variety of mechanisms. Most simply, crystallites serve as impenetrable obstacles which diminish the volume available for transport. When the volume fraction of crystallites becomes high enough, tortuosity effects can become important. It is also believed that the presence of crystallite anchoring points can constrain relaxations in the amorphous phase and so reduce the ability of penetrating molecules to squeeze through. In the case of these polyimides in which the levels of crystallinity are very small and the experiments are performed over 200 deg below the material glass transitions, it is reasonable to assume that only the first mechanism is operative.

As we have indicated, the PMDA/ODA samples which were processed below the material glass transitions are less dense than what we estimate for a dense amorphous state. Okamoto et al.[1] showed that the diffusivity of water through various polyimides could be correlated by a so-called "fractional free space" in the material, which is the ratio of the difference of the measured specific volume and the hard sphere volume to the measured specific volume. Hard sphere volumes were calculated from a group contribution approach. Although quite similar in

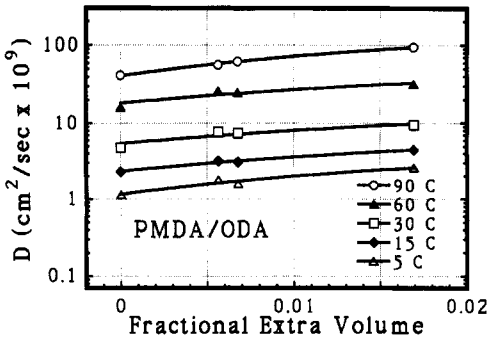

Figure 15. Dependence of the measured diffusion coefficients on the "fractional extra volume" in the polymer glass.

Table 3. Free Energy Differences by Cluster Size

n (molecules/cluster)	ΔG (kcal/mol)	n (molecules/cluster)	ΔG (kcal/mol)
2	1.33	4	2.48
3	1.90	5	3.05

concept, we have chosen to define our fractional free volume using only experimentally obtainable parameters:

$$\frac{V^{obs} - V^{dens}}{V^{dens}} \tag{6}$$

where V^{dens} represents the volume of a dense amorphous phase and V^{obs} is the experimentally determined sample density. Figure 15 illustrates the dependence of the measured diffusion coefficients of D_2O in PMDA/ODA on this parameter. (In this figure, the coefficient for the one semicrystalline sample was normalized by the volume fraction of the amorphous phase.) It is apparent that the diffusivity of the penetrant increases dramatically as the glassy phase becomes less dense.

The differences in amorphous densities achievable in these glasses is quite remarkable. It is illustrative to calculate the hydrostatic pressure that would be required to achieve equivalent differences, which is readily calculable using the material isothermal compressibility. For PMDA/ODA, the compressibility near room temperature is ca. 2×10^{-4} MPa^{-1}.[14] Table 1 shows that the lowest density sample is "expanded" from the dense state by 1.7%, which would therefore be equivalent to a negative pressure on the order of 85 MPa (120 000 psi).

As discussed previously, we are currently unable to quantitatively compare the diffusion in the two BPDA/PPD samples due to an inability to calculate the volume fraction of the amorphous phase. All that can be said is that the more highly crystalline sample does show a markedly lower diffusivity.

For the BTDA/ODA//MPD copolymer, in which there is no crystallinity, the diffusion coefficients in the two samples were found to be the same within experimental error.

Effect of Orientation and Chain Stiffness. The measured diffusivities increase in the order BPDA/PPD < BTDA/PPD < PMDA/ODA ~ BTDA/ODA//MPD. This approximately mimics the decrease in local backbone stiffness as measured by the temperature of the mechanical β transition, which is presented in Table 3. The activation energies for diffusion decreased in the order BTDA/PPD > BPDA/PPD > PMDA/ODA > BTDA/ODA//MPD. These results show that there is a significant difference in the ability for water to squeeze between chains, even for chains of similar backbone composition in the glassy state. It would appear plausible that the activation energy for penetrant diffusion should increase with increasing chain stiffness, which would make it more difficult for the requisite small interchain displacements to occur. Unfortunately, it is not possible to correlate the activation energies with either the temperature or activation energy for the mechanical β transitions of these materials.

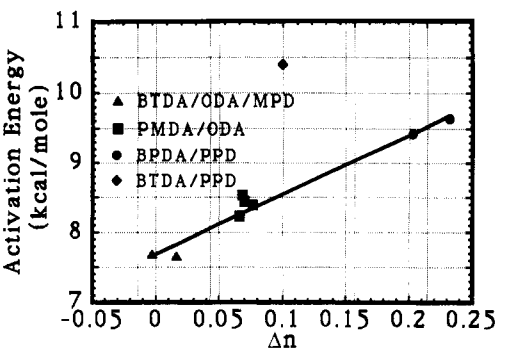

Figure 16. Relationship between the birefringence and the activation energy for water diffusion.

A second possibility is that the activation energy for penetrant diffusion might be related to orientation within the polyimide film. It has become well established that the in-plane coefficient of thermal expansion (CTE) is directly related to the planarity (or birefringence) of the polyimide chains, with the CTE decreasing dramatically as the planarity of molecules in the film increases.[3] Since the in-plane CTE is a direct measurement of the ease with which interchain spacings increase with temperature, it is plausible that the temperature dependence of the through-plane diffusion might be sensitive to it. Figure 16 shows that this explanation is also incomplete, since the behavior of the BTDA/PPD composition deviates significantly from this correlation.

We are therefore left without an easy link between chain stiffness or the morphology of the sample and the measured activation energies. A complete description of small molecule diffusion in these glasses would require some coupling of chain orientation with the changing distribution and amplitude of chain motions with temperature. This is out of the scope of the present work.

State of the Absorbed Water. As discussed previously, the infrared spectra clearly show that at saturation the water appears to be partitioned between two distributions of hydrogen bonded environments. Our analysis of the spectra indicate that in one environment the water exists in a monomeric form, albeit hydrogen bonded to the chain backbone, and that the other environment is probably an aggregate with an average population of three water molecules. At 30 °C, approximately 77% of the total exists in the aggregated form. These results are in superb agreement with the NMR studies of Xu et al.,[2] which concluded that ca. 70% of the absorbed water existed in clusters consisting of a small number of water molecules. Our analysis of the equilibrium distribution between these two sites shows that the energy difference between them, ca. 2 kcal/mol, is reasonably small and well within the range of what would be expected for a hydrogen bonded system.[12]

At the earliest times, where the polymer matrix is far from saturation, the site distribution is quite different. As shown in Figure 17, in PMDA/ODA the distribution is centered around 2645 cm^{-1} with a trimodal distribution. This trimodal distribution is quickly washed out by the dominant bimodal distribution discussed previously. It is apparent that the partitioning of the absorbed water molecules is a very sensitive probe of the level of local heterogeneity of the polyimide glass.

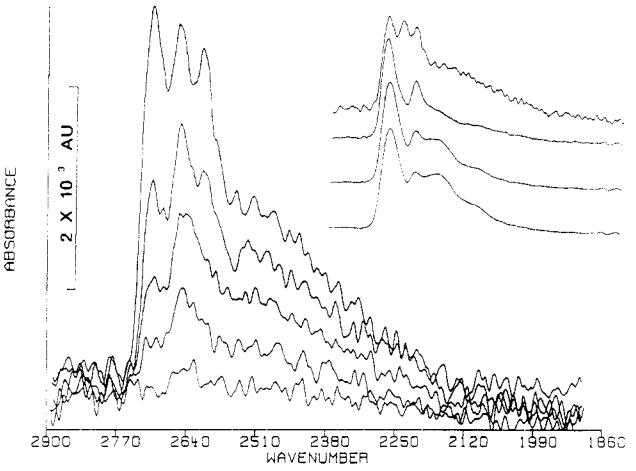

Figure 17. Illustration of the change in the site distribution of the absorbed D_2O molecules as absorption proceeds. From the bottom, the spectra were acquired at uptakes of 0.0019, 0.0051, 0.0106, 0.0176, and 0.0258. The inset continues this progression to later times; from the top, spectra were acquired at uptakes of 0.0258, 0.124, 0.61, and 1.

Conclusions

We have studied the differences in the transport behavior of water in glassy polyimide films based on cure conditions and backbone chemistry. The predominant determinants of the diffusion behavior have been found to be chain stiffness, the level of crystallinity, and the density of the amorphous phase. The activation energies for diffusion were found not to easily correlate to any measurement of the chain stiffness or orientation, and probably reflect a complex convolution of the two.

The vibrational spectra of the absorbed water was also found to be remarkably sensitive to the environment and are indicative of two dominant distributions of environments at saturation. At levels well below saturation absorbed water partitions into at least three distinct environments, indicative of the very high degree of inhomogeneity that exists in these materials.

Acknowledgment. We thank KennCorwin Gardner, Michael Pottiger, Brian Cox, and Kyle Cope for their important contributions to this work.

References and Notes

(1) Okamoto, K.; Tanihara, N.; Watanabe, H.; Tanaka, K.; Hidetoshi, K.; Nakamura, A.; Kusuki, Y.; Nakagawa, K. *J. Polym. Sci., Part B: Polym. Phys.* **1992**, *30*, 1223. Moylan, C. R.; Best, M. E.; Ree, M. *J. Polym. Sci., Part B: Polym. Phys.* **1991**, *29*, 87. Yang, D. K.; Koros, W. J.; Hopfenberg, H. B.; Stannet, V. T. *J. Appl. Polym. Sci.* **1986**, *31*, 1619. Yang, D. K.; Koros, W. J.; Hopfenberg, H. B.; Stannet, V. T. *J. Appl. Polym. Sci.* **1985**, *30*, 1035. Denton, D. D.; Day, D. R.; Priore, D. F.; Senturia, S. D. *J. Electron. Mater.* **1985**, *14*, 119. Sacher, E.; Susko, J. R. *J. Appl. Polym. Sci.* **1981**, *26*, 679. Sacher, E.; Susko, J. R. *J. Appl. Polym. Sci.* **1979**, *23*, 2355.

(2) Lim, B. S.; Nowick, A. S.; Lee, K.; Viehbeck, A. *J. Polym. Sci., Part B: Polym. Phys.* **1993**, *31*, 545. Xu, G.; Gryte, C. C.; Nowick, A. S.; Li, S. Z.; Pak, Y. S.; Greenbaum, S. G. *J. Appl. Phys.* **1989**, *66*, 5290. Melcher, J.; Daben, Y.; Arlt, G. *IEEE Trans. Electr. Insul.* **1989**, *24*, 31.

(3) Coburn, J. C.; Pottiger, M. T. *Proc. Int. Conf. Polyimides, 4th*, **1991**.

(4) Hemmelman, V. K.; Brandt, H. *Exp. Tech. Phys.* **1989**, *37*, 495.

(5) Fieldson, G. T.; Barbari, T. A. *Polymer* **1993**, *34*, 1146.

(6) Harrick, N. J. *Internal Reflection Spectroscopy*; John Wiley & Sons: New York, 1967.

(7) Crank, J. *The Mathematics of Diffusion*; Oxford University Press: Oxford, U.K., 1956.

(8) Gardner, K. H. Personal communication.

(9) Noe, S. C.; Pan, J. Y.; Senturia, S. D. *Proceedings of the 49th Annual Technical Conference*, Montreal, Quebec, Canada; Society of Plastics Engineers: Brookfield, CT, 1991; p 1598.

(10) Pacansky, J.; England, C.; Waltman, R. J. *J. Polym. Sci., Part B: Polym. Phys.* **1987**, *25*, 901.

(11) Salzberg, C. D. *J. Opt. Soc. Am.* **1957**, *47*, 244.

(12) Pimentel, G. C.; McClellan, A. L. *The Hydrogen Bond*; Reinhold Publishing: New York, 1960.

(13) Yoon, D. Y.; Parrish, W.; Depero, L. E.; Ree, M. *Mater. Res. Soc. Symp. Proc.* **1991**, *227*, 387.

(14) Dee, G. T. Data to be published.